MAGNETIC RESONANCE

Identification of high-risk carotid plaque with MRI-based radiomics and machine learning

Ranying Zhang[1] · Qingwei Zhang[2] · Aihua Ji[1] · Peng Lv[1] · Jingjing Zhang[1] · Caixia Fu[3] · Jiang Lin[1]

Abstract

Objectives We sought to build a high-risk plaque MRI-based model (HRPMM) using radiomics features and machine learning for differentiating symptomatic from asymptomatic carotid plaques.

Materials and methods One hundred sixty-two patients with carotid stenosis were randomly divided into training and test cohorts. Multi-contrast MRI including time of flight (TOF), T1- and T2-weighted imaging, and contrast-enhanced imaging was done. Radiological characteristics of the carotid plaques were recorded and calculated to build a traditional model. After extracting the radiomics features on these images, we constructed HRPMM with least absolute shrinkage and selection operator algorithm in the training cohort and evaluated its performance in the test cohort. A combined model was also built using both the traditional and radiomics features. The performance of all the models in the identification of high-risk carotid plaque was compared.

Results Intraplaque hemorrhage and lipid-rich necrotic core were independently associated with clinical symptoms and were used to build the traditional model, which achieved an area under the curve (AUC) of 0.825 versus 0.804 in the training and test cohorts. The HRPMM and the combined model achieved an AUC of 0.988 versus 0.984 and of 0.989 versus 0.986 respectively in the two cohorts. Both the radiomics model and combined model outperformed the traditional model, whereas the combined model showed no significant difference with the HRPMM.

Conclusions Our MRI-based radiomics model can accurately distinguish symptomatic from asymptomatic carotid plaques. It is superior to the traditional model in the identification of high-risk plaques.

Key Points
• *Carotid plaque multi-contrast MRI stores other valuable information to be further exploited by radiomics analysis.*
• *Radiomics analysis can accurately distinguish symptomatic from asymptomatic carotid plaques.*
• *The radiomics model is superior to the traditional model in the identification of high-risk plaques.*

Keywords Magnetic resonance imaging · Stroke · Atherosclerotic plaques · Carotid artery · Machine learning

Abbreviations

AUC	Area under the curve
CER	Contrast enhancement ratio
GLCM	Gray-level co-occurrence matrix
GLDM	Gray-level dependence matrix
GLRLM	Gray-level run-length matrix

Ranying Zhang and Qingwei Zhang contributed equally to this work.

Electronic supplementary material The online version of this article (https://doi.org/10.1007/s00330-020-07361-z) contains supplementary material, which is available to authorized users.

✉ Jiang Lin
  lin.jiang@zs-hospital.sh.cn

1 Department of Radiology, Zhongshan Hospital, Fudan University and Shanghai Institute of Medical Imaging, 180 Fenglin Road, Shanghai 200032, China

2 Division of Gastroenterology and Hepatology, Key Laboratory of Gastroenterology and Hepatology, Ministry of Health, Renji Hospital, School of Medicine, Shanghai Jiao Tong University, Shanghai Institute of Digestive Disease, 145 Middle Shandong Road, Shanghai, China

3 MR Application Development, Siemens Shenzhen Magnetic Resonance Ltd., Gaoxin C. Ave, 2nd, Hi-Tech Industrial Park, Shenzhen 518057, China

GLSZM   Gray-level size-zone matrix
HRPMM   High-risk plaque MRI-based model
ICC   Intraclass coefficient
IPH   Intraplaque hemorrhage
LASSO   Least absolute shrinkage and selection operator
LRNC   Lipid-rich necrotic core
MLA   Minimal luminal area
MRI   Magnetic resonance imaging
NDLR   Negative diagnostic likelihood ratio
NPV   Negative predictive value
PB   Plaque burden
PDLR   Positive diagnostic likelihood ratio
PPV   Positive predictive value
RI   Remodeling index
ROC   Receiver operating characteristic
TOF   Time of flight
VIBE   Volume-interpolated breath-hold examination

Carotid atherosclerosis is a major cause of ischemic stroke accounting for approximately 18–25% of all strokes [1]. Disease severity and risk of stroke are traditionally determined by luminal stenosis and surface irregularities. However, many recent studies have suggested the critical importance of identifying vulnerable plaques by determining their compositions [2, 3], due to their correlation with higher risks of cerebral infarction. Multi-contrast MR imaging (MRI) has been established as an effective method for plaque characterization. Major relevant applications include the diagnosis of intraplaque hemorrhage (IPH) [4] and lipid-rich necrotic core (LRNC), both of which are high-risk features associated with cerebrovascular events. Despite its reliability and noninvasiveness, MR plaque imaging is complex and requires expertise in assessing various plaque components which is a qualitative and subjective task in nature. Radiomics is a computing process of extracting and analyzing large number of quantitative features from medical images. The success of radiomics rests on the assumption that medical images contain additional information which may not be obvious under visual inspection [5]. It has proven to be a valuable tool in oncology, including diagnosis, staging, and grading of cancer; assessment of treatment response; and prediction of clinical outcomes [6–9]. Recently CT- or ultrasound-based texture analysis has been employed to discriminate symptomatic carotid plaques with promising results [10, 11]. Compared with CT and ultrasound, high-resolution MR plaque imaging provides inherently superior soft tissue contrasts, and a combination of multiple contrast weightings potentially confers more valuable information. Additional advantages of MRI include its lack of radiation and operator-independence. However, up until today, there is no data available regarding MR radiomics on carotid plaque, except for one initial report on MR texture analysis of basilar artery plaque [12].

The purpose of this study was to build a high-risk plaque MRI-based model (HRPMM) using a radiomics approach combined with machine learning and to evaluate its performance in differentiating symptomatic from asymptomatic carotid plaques by comparing it with traditional MR features.

Materials and methods

Patients

We retrospectively collected 217 patients from January 2015 to June 2019, who had carotid stenosis of > 30% diagnosed by ultrasound or angiography (NASCET criteria [13]). These patients underwent both carotid plaque MRI and head MRI within the same day. The study was approved by the ethics committee of our institution and informed consent was obtained from all patients.

All patients were divided into symptomatic and asymptomatic groups according to whether they had clinical symptoms within 2 weeks before the MRI examination and/or whether their head MRI showed acute/subacute stroke [14, 15]. The clinical symptoms included classic TIA (transient ischemic attack) and ischemic stroke in the anterior circulation (carotid territory) [16, 17], as well as monocular symptoms (amaurosis fugax or retinal artery occlusion) ipsilateral to the carotid plaque [18]. Classic TIA was defined as an abnormal focal neurologic deficit lasting less than 24 h. A complete ischemic stroke presented with an abrupt onset of a focal neurologic deficit lasting > 24 h [17]. Clinical characteristics were recorded including gender, age, and atherosclerotic risk factors (hypertension, diabetes, hyperlipidemia, and cigarette smoking).

The exclusion criteria were as follows: (a) evidence of cardiogenic stroke; (b) bilateral TIA/stroke, brainstem involvement only or undetermined hemispheric involvement; (c) primary intracranial diseases; (d) radiotherapy-induced carotid stenosis; (e) contraindications to MRI (such as pacemaker or severe claustrophobia) or to gadolinium. In total, 55 patients were excluded and 162 patients were finally included in this study. Eligible patients were randomly divided into a training cohort ($n = 121$) and an independent test cohort ($n = 41$) in a ratio of 3:1. From all these enrolled patients with carotid stenosis, if a carotid plaque was found in one with clinical symptoms or positive head MRI findings, it was classified as a symptomatic plaque; otherwise, it was asymptomatic.

Magnetic resonance imaging

All patients were scanned on a 3-T MR scanner (MAGNETOM Verio, Siemens Healthineers) with a 16-channel head coil and an 8-channel carotid coil. The following carotid MR pulse sequences were applied to obtain the cross-sectional images centered at the carotid bifurcation: (a) 3D

time-of-flight (TOF), (b) T1W turbo spin-echo (TSE), (c) T2W TSE, (d) dynamic contrast-enhanced 3D volume-interpolated breath-hold examination (DCE 3D VIBE), (e) post-contrast delayed T1W TSE.

Gadopentetate dimeglumine (Magnevist, Bayer) was used for DCE plaque imaging with a dosage of 0.1 mmol/kg body weight followed by a 20-ml saline flush through an 18-G venous catheter positioned in an antecubital vein. The contrast material was injected by a power injector at an injection rate of 2 ml/s. The DCE acquisition was repeated 16 times continuously with each acquisition of 18 s. The 2nd acquisition was initiated synchronously with the start of the contrast administration. Post-contrast delayed imaging was done immediately after DCE acquisition. Detailed imaging parameters are in Table 1. The total scan time was approximately 22 min.

Image analysis and segmentation

Traditional measurements and analysis were performed on a workstation (Syngo; Siemens Healthineers) by a radiologist with 4 years of experience in plaque imaging. The slice with the largest plaque area was chosen to be measured. The inner lumen and outer wall boundaries were manually outlined on T1WI to measure the plaque burden (PB), minimal luminal area (MLA), remodeling index (RI), and contrast enhancement ratio (CER). The related calculation formulas were as follows:

$$PB = \left(1 - \frac{lumen\ area}{vessel\ area}\right) \times 100\%;$$

$$RI = \left(\frac{vessel\ area\ at\ the\ point\ of\ maximum\ stenosis}{reference\ vessel\ area\ at\ the\ distal\ portion}\right);$$

$$CER = \left(\frac{(signal\ of\ plaque\ [post-contrast\ delayed])}{(signal\ of\ plaque\ [pre-contrast\ T1WI])} - 1\right) \times 100\%.$$

The degree of stenosis was measured on T1WI according to the NASCET criteria [13]. Plaque major components including IPH and LRNC were identified and recorded too [19, 20]. Disrupted luminal surface was identified as a deficit in the fibrous cap or discontinuous surface of the plaque [17].

Plaque segmentation for radiomics analysis was performed with an open-source software ITK-SNAP (version 3.8.0, www.itk-snap.org). After choosing the slice showing the largest plaque on different sequences including T1W, T2W, DCE, and post-contrast delayed T1W, regions of interest (ROIs) were manually drawn by the same radiologist along the margin of the plaques. For the DCE sequence, we drew ROI on the 5th phase image due to its highest signal intensity in the carotid lumen at that phase. Sample patient images were shown in Fig. 1.

Feature extraction, selection, and model development

Of all the radiological variables from 162 patients, we chose those with $p < 0.05$ in univariate tests to perform multivariable logistic regression analysis and calculated the odds ratios (ORs) with 95% confidence intervals (CIs). The variables with $p < 0.05$ in multivariate analysis were finally used to build a linear traditional model.

Before radiomics feature extraction, all MRI images were subjected to imaging normalization (the intensity of the image was scaled to 0–100) and resampled to the same resolution (2 mm × 2 mm × 2 mm) to avoid data heterogeneity bias. Radiomics features were then extracted on PyRadiomics platform [21, 22]. For each ROI on each sequence, a wavelet filter was applied.

To build a predictive radiomics model for identifying high-risk plaques, the following steps were done. Firstly, the meth-

Table 1 Summery of imaging parameters for the multi-contrast MRI protocol

Sequence	Carotid plaque MRI					Head MRI			
	T1W	T2W	TOF	DCE	POST	Axial T1W	Axial T2W	DWI	FLAIR
FOV (mm)	160 × 160	160 × 160	160 × 160	160 × 160	160 × 160	220 × 220	220 × 220	220 × 220	220 × 220
Matrix	256 × 256	256 × 256	256 × 256	256 × 256	256 × 256	320 × 240	384 × 307	164 × 164	256 × 217
Slice thickness (mm)	2	2	2	2	2	5	5	5	5
Resolution (mm^2)	0.63 × 0.63	0.63 × 0.63	0.63 × 0.63	0.63 × 0.63	0.63 × 0.63	0.9 × 0.7	1.0 × 0.9	1.3 × 1.3	1.0 × 0.9
TR/TE (ms)	700/9.4	4000/59	26/3.23	5.07/4.79	700/9.4	2000/18	6000/100	6400/86	9000/94
NEX	2	2	1	1	2	1	1	1	1
Bandwidth (Hz/pixel)	407	407	250	390	407	260	221	1172	287
Flip angle (°)	160	160	25	12	160	150	150	/	150
Acquisition time	3 min 34 s	3 min 06 s	2 min 33 s	4 min 52 s	3 min 34 s	1 min 14 s	50 s	48 s	1 min 32 s

TOF, time of flight; *DCE*, dynamic contrast-enhanced sequence; *POST*, post-contrast delayed sequence; *DWI*, diffusion-weighted imaging; *FLAIR*, fluid-attenuated inversion recovery; *FOV*, field of view; *TR*, repetition time; *TE*, echo time; *NEX*, number of excitations
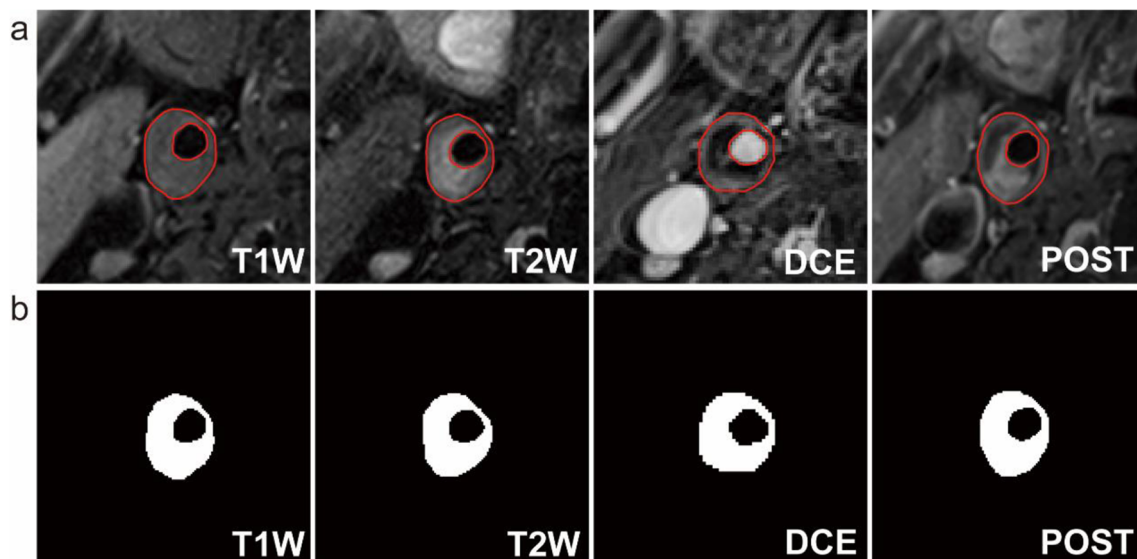
Fig. 1 The procedure of radiomics segmentation. **a** In one patient with the regions of interest (ROIs) outlining the carotid plaque on T1W, T2W, DCE (dynamic contrast-enhanced), and POST-contrast delayed images. **b** The segmentations extracted from the ROIs corresponding to the images on **a**

od of normalization to z distribution ([value − mean value]/ standard deviation) was applied for each extracted feature. Secondly, t tests were used to select the features with $p < 0.05$ in each sequence, and then the features with significant differences and an area under the curve (AUC) > 0.65 by receiver operating characteristic (ROC) were selected. Thirdly, the least absolute shrinkage and selection operator (LASSO) algorithm was applied for further feature reduction. The most significant features with the smallest deviance were then selected using the LASSO algorithm for the final features. The LASSO algorithm is a penalized regression method which has been successfully applied to some oncologic researches [8, 9, 23, 24]. The LASSO algorithm can estimate the regression coefficients by maximizing the log-likelihood function (or the sum of squared residuals) with the constraint, reduce the coefficients of indistinctive covariates to zero, and enable the non-zero features to be combined into a radiomics model [23]. Using these final features after the LASSO algorithm, we constructed a linear radiomics model called high-risk plaque MRI-based model (HRPMM) in the training cohort and then evaluated its performance in the test cohort. With this model, the risk score for each patient was calculated by a formula weighted by regression coefficients: Risk score = constant + coefficients × features. To determine the optimal cutoff value to classify the plaques into low- and high-risk, the R software was used to calculate the Youden index for all possible cutoff values (c) (Youden index = maxc {Sensitivity + Specificity − 1 }), and the value of c that achieves the maximized index will be considered the optimal one [25].

Finally, a combined model was built based on the multivariate logistic regression analysis in the R software combining both the traditional and radiomics features (flow chart in Fig. 2).

The inter-observer agreement

To evaluate the reproducibility of the radiological and radiomics analysis, another radiologist with 7 years' experience in plaque imaging independently completed the plaque analysis in 40 patients who were randomly selected from the study population.

Statistical analysis

All statistical analyses were performed using the R software (version 3.5.0) and IBM SPSS Statistics 23.0. Univariate analysis was performed to assess the relationship between each variable and symptomatic status, t test was used for continuous variables, and the Chi-squared test or Fisher's exact test was for the categorical variables. Variables with statistical significance in the univariate analysis were used in the multivariate logistic analysis. The clinical characteristics of the training and test cohorts were compared appropriately using t test, Fisher's exact test, or Chi-squared test. A two-tailed p value of < 0.05 was considered statistically significant.

A nomogram of the combined model was established by the R software. For each model, AUC values were calculated using ROC analysis to assess the predictive ability. Accuracy, sensitivity, specificity, negative predictive value (NPV), positive predictive value (PPV), positive diagnostic likelihood ratio (PDLR), and

Fig. 2 Flow chart for building the models in the identification of high-risk plaques
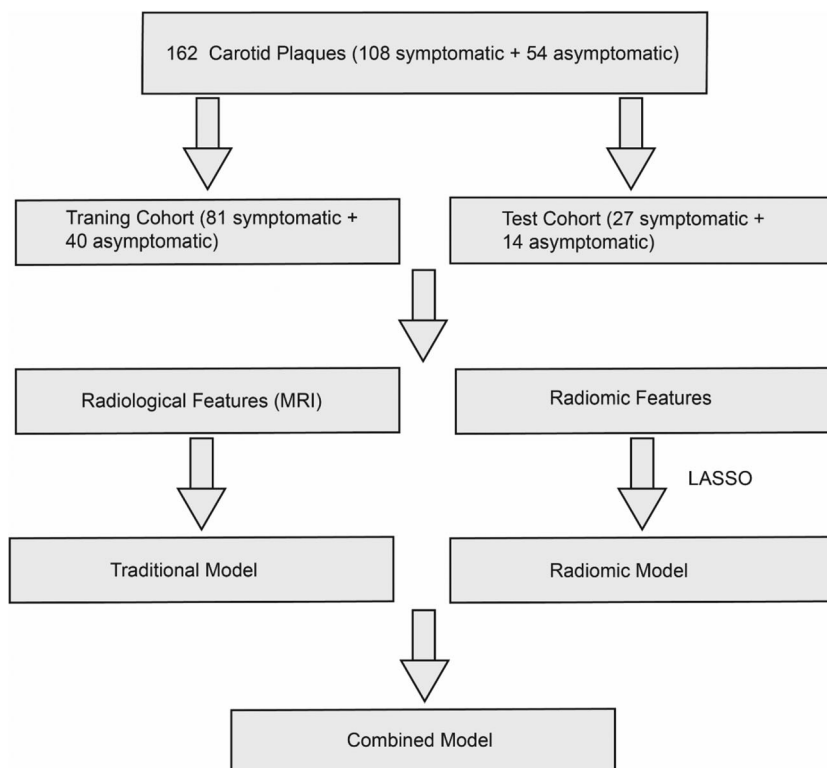
negative diagnostic likelihood ratio (NDLR) were also measured using the defined optimal cutoff values. The Delong method was used for comparing the AUCs of all these models [9].

Table 2 Clinical and radiological characteristics of the carotid plaques

	n/total (%)	Symptomatic	Asymptomatic	p value[b]	Multivariate OR (95 %CI)[c]	p value[c]	AUC
Gender	162	108	54	0.166[d]	/	/	
Male	148 (91.4)	101	47				
Female	14 (8.6)	7	7				
Age [a]	66.80 ± 7.37	66.41 ± 7.02	67.52 ± 7.96	0.367[e]	/	/	
Hypertension	124 (76.5)	80	44	0.294[d]	/	/	
Diabetes mellitus	56 (34.6)	38	18	0.815[d]	/	/	
Hyperlipidemia	74 (45.7)	61	13	<0.001[d]	2.497 (0.938, 6.643)	0.067	
Smoking	53 (32.7)	35	18	0.906[d]	/	/	
IPH	53 (32.7)	49	4	<0.001[f]	7.568 (1.933, 26.627)	0.004	0.708
LRNC	84 (51.9)	71	13	<0.001[d]	3.835 (1.409, 10.441)	0.009	0.690
Disrupted surface	27 (16.7)	23	4	0.026[f]	1.619 (0.375, 7.002)	0.519	
MLA (cm²) [a]	0.19 ± 0.16	0.14 ± 0.14	0.28 ± 0.15	<0.001[e]	0.325 (0.002, 47.884)	0.659	
Degree of stenosis (%)[a]	59.69 ± 20.30	67.33 ± 19.55	44.95 ± 12.88	<0.001[e]	25.291 (0.341, 1873.499)	0.141	
Enhancement ratio (%)[a]	60.92 ± 67.51	42.26 ± 56.71	98.22 ± 72.27	<0.001[e]	0.566 (0.267, 1.199)	0.137	
Plaque burden (%)[a]	78.12 ± 15.20	84.03 ± 13.08	67.43 ± 12.85	<0.001[e]	83.978 (0.229, 849.463)	0.141	
Remodeling index [a]	1.22 ± 0.27	1.26 ± 0.27	1.15 ± 0.24	0.009[e]	6.579 (0.818, 52.940)	0.077	

AUC, area under the curve; *CI*, confidence intervals; *IPH*, intraplaque hemorrhage; *LRNC*, lipid-rich necrotic core; *MLA*, minimum luminal area; *OR*, odds ratio

[a] Continuous variables shown with mean ± standard deviation (SD), others are categorical variables; [b] Univariate analysis; [c] Results from multivariate logistic analysis; [d] Chi-squared test; [e] *T* test; [f] Fisher exact test

To correct overfitting bias, corrected AUCs were calculated using bootstrapping validation (1000 bootstrap resamples) in the training cohort. Intraclass coefficients (ICCs) were calculated for the inter-observer agreement [9]: ICC < 0.40, poor agreement; 0.41–0.60, moderate; 0.61–0.80, substantial; and > 0.80, excellent.

Results

Patient characteristics

Of all the 162 enrolled patients, there were 108 symptomatic and 54 asymptomatic patients. The clinical and radiological characteristics are listed in Table 2. These characteristics in the training and test cohorts show no significant difference in Table 3.

Traditional assessment of the carotid plaques

Univariate analysis showed that hyperlipidemia, IPH, LRNC, disrupted surface, MLA, degree of stenosis, PB, CER, and RI were associated with symptomatic plaques ($p < 0.05$, Table 2). Multivariate logistic regression analysis showed that IPH (OR = 7.568; 95% CI, 1.933–26.627) and LRNC (OR = 3.835; 95% CI, 1.409–10.441) were independent predictors of clinical symptoms. In the training cohort, the AUC values of

Table 3 Clinical and radiological characteristics in the training and test cohort

	Training cohort (N = 121)	Test cohort (N = 41)	p value
Gender			1.000 [a]
Male	110 (90.9%)	38 (92.68%)	
Female	11 (9.1%)	3 (7.32%)	
Age	67.09 ± 6.98	65.93 ± 8.44	0.590 [b]
Hypertension			0.490 [c]
Yes	91 (75.21%)	33 (80.49%)	
No	30 (24.79%)	8 (19.51%)	
Diabetes mellitus			0.656 [c]
Yes	43 (35.54%)	13 (31.71%)	
No	78 (64.46%)	28 (68.29%)	
Hyperlipidemia			0.792 [c]
Yes	56 (46.28%)	18 (43.90%)	
No	65 (53.72%)	23 (56.10%)	
Smoking			0.167 [c]
Yes	36 (29.75%)	17 (41.46%)	
No	85 (70.25%)	24 (58.54%)	
IPH			0.586 [c]
Yes	41 (33.88%)	12 (29.27%)	
No	80 (66.12%)	29 (70.73%)	
LRNC			0.789 [c]
Yes	62 (51.24%)	22 (53.66%)	
No	59 (48.76%)	19 (46.34%)	
Disrupted surface			0.419 [c]
Yes	18 (14.88%)	9 (21.95%)	
No	103 (85.12%)	32 (78.05%)	
MLA (cm^2)	0.19 ± 0.17	0.17 ± 0.15	0.473 [b]
Degree of stenosis (%)	59.47 ± 20.05	61.03 ± 22.01	0.823 [b]
Enhancement ratio (%)	60.00 ± 66.48	61.23 ± 71.24	0.797 [b]
Plaque burden (%)	77.48 ± 15.40	81.48 ± 14.16	0.135 [b]
Remodeling index	1.21 ± 0.24	1.26 ± 0.32	0.327 [b]

[a] Fisher exact test; [b] T test; [c] Chi-squared test

IPH, intraplaque hemorrhage; *LRNC*, lipid-rich necrotic core; *MLA*, minimum luminal area

IPH and LRNC were 0.697 and 0.715 respectively; the AUC value was improved to 0.825 when combining IPH and LRNC. In the test cohort, the above values were 0.668, 0.690, and 0.804 (Table 4).

Radiomics analysis of the carotid plaques

From each ROI on each sequence, we extracted 788 radiomics features on both the original and filtered images, including 18

Table 4 Predictive ability of all models

	Sensitivity (%)	Specificity (%)	Accuracy (%)	AUC	NPV (%)	PPV (%)	PDLR	NDLR
Traditional model—training cohort (n = 121)								
LRNC	85.48	54.24	70.25	0.715	78.05	66.25	1.87	0.27
IPH	92.68	47.50	62.81	0.697	92.68	47.50	1.76	0.15
All	86.25	70.73	80.99	0.825	72.50	85.15	2.95	0.19
Traditional model—test cohort (n = 41)								
LRNC	81.82	52.63	65.85	0.690	71.43	66.67	1.73	0.34
IPH	91.67	44.83	58.54	0.668	92.85	40.74	1.66	0.18
All	85.19	71.43	80.49	0.804	71.43	85.19	2.98	0.20
Radiomics model—training cohort (n = 121)								
T1W	88.06	77.42	84.69	0.861	75.00	89.39	3.9	0.15
T2W	83.58	80.65	82.65	0.869	69.44	90.32	4.32	0.2
DCE	89.55	77.42	85.71	0.907	77.42	89.55	3.97	0.13
Post	76.12	93.55	81.63	0.890	64.44	96.22	11.79	0.25
All	92.54	96.77	93.88	0.988	85.71	98.41	28.68	0.08
Radiomics model—test cohort (n = 41)								
T1W	92.59	57.14	80.48	0.894	80.00	80.64	2.16	0.13
T2W	85.18	85.71	89.19	0.897	75.00	92.00	5.96	0.17
DCE	66.67	92.85	75.61	0.965	57.09	94.74	9.33	0.36
POST	88.89	92.85	90.24	0.978	81.25	92.86	12.44	0.12
All	81.48	100.00	90.49	0.984	74.68	100.00	/	0.18
Combined model—training cohort (n = 121)								
Combined_ T1W	91.04	77.42	86.73	0.867	80.00	89.70	4.03	0.11
Combined_ T2W	88.06	77.42	84.69	0.877	75.00	89.39	3.90	0.15
Combined_ DCE	100	77.42	92.85	0.935	100	90.54	4.43	0
Combined_ Post	86.57	87.10	86.73	0.899	75.00	93.54	6.71	0.015
Combined_ All	92.53	96.77	93.88	0.989	85.71	98.41	28.68	0.08
Combined model—test cohort (n = 41)								
Combined_ T1W	88.89	78.57	85.36	0.892	78.57	88.89	4.15	0.14
Combined_ T2W	77.78	92.85	82.93	0.912	68.42	95.45	10.89	0.23
Combined_ DCE	92.59	85.71	90.24	0.970	85.71	92.59	6.48	0.09
Combined_ Post	92.59	78.57	87.80	0.958	84.61	89.28	4.32	0.09
Combined_ All	92.60	92.86	92.68	0.986	86.67	96.15	12.96	0.08

AUC, area under curve; *NPV*, negative predictive value; *PPV*, positive predictive value; *PDLR*, positive diagnostic likelihood ratio; *NDLR*, negative diagnostic likelihood ratio; *DCE*, dynamic contrast-enhanced sequence; *POST*, post-contrast delayed sequence; *All*, all features of the corresponding models; /, default value, unable to calculate specific value because of the 100% of specificity

features of first-order statistics, 14 features of shape, 68 features of texture (22 gray-level co-occurrence matrix (GLCM) features, 16 gray-level run-length matrix (GLRLM) features, 16 gray-level size-zone matrix (GLSZM) features, 14 gray-level dependence matrix (GLDM) features), and 688 features of wavelet. In total, 510,624 radiomics features were extracted from all ROIs, and we selected 387 features with significant association with clinical symptoms, including 85, 68, 72, and 162 radiomics features from T1W, T2W, DCE, and post-contrast delayed images respectively. After the LASSO algorithm was applied, 33 features were finally retained and used to build HRPMM (details are shown in the Appendix).

In the training cohort of HRPMM, radiomics features on T1W, T2W, DCE, and post-contrast delayed images had AUC values of 0.861, 0.869, 0.907, and 0.890, while AUC values of the test cohort were 0.894, 0.897, 0.965, and 0.978. When combining four sequences, in the training cohort, the AUC value reached 0.988 with a sensitivity of 92.54%, specificity of 96.77%, and accuracy of 93.88%; in the test cohort, the AUC was 0.984 with a sensitivity of 81.48%, specificity of 100%, and accuracy of 90.49% (Table 4).

A combined model was finally constructed and shown as a nomogram (Fig. 3). This combined model exhibited an AUC value of 0.989 in the training cohort and 0.986 in the test cohort (Table 4). The ROC curves of the HRPMM and the

combined model outperformed those of the traditional model in the training cohort ($p = 0.000$, $p = 0.000$) and test cohort ($p = 0.021$, $p = 0.020$). However, the combined model showed no significant difference with the HRPMM in the two cohorts ($p = 0.798$, $p = 1.000$) (Fig. 4).

The corrected AUCs from resamples in the training cohort were as follows: T1WI (0.860), T2WI (0.863), DCE (0.906), post-contrast delayed (0.890), and all sequences (0.988), which were close to those of the radiomics model in Table 4.

The inter-observer agreement

The ICCs for measuring the radiological and radiomics features ranged from 0.705 to 0.951 and were summarized in the Appendix.

Discussion

With the risk of ipsilateral cerebrovascular events caused by carotid atherosclerosis, a considerable number of MRI studies on carotid plaque have been performed to search for relevant plaque components or characteristics. While previous studies were mostly focused on the traditional evaluation of the plaques, in this study, we used a radiomics approach to extract
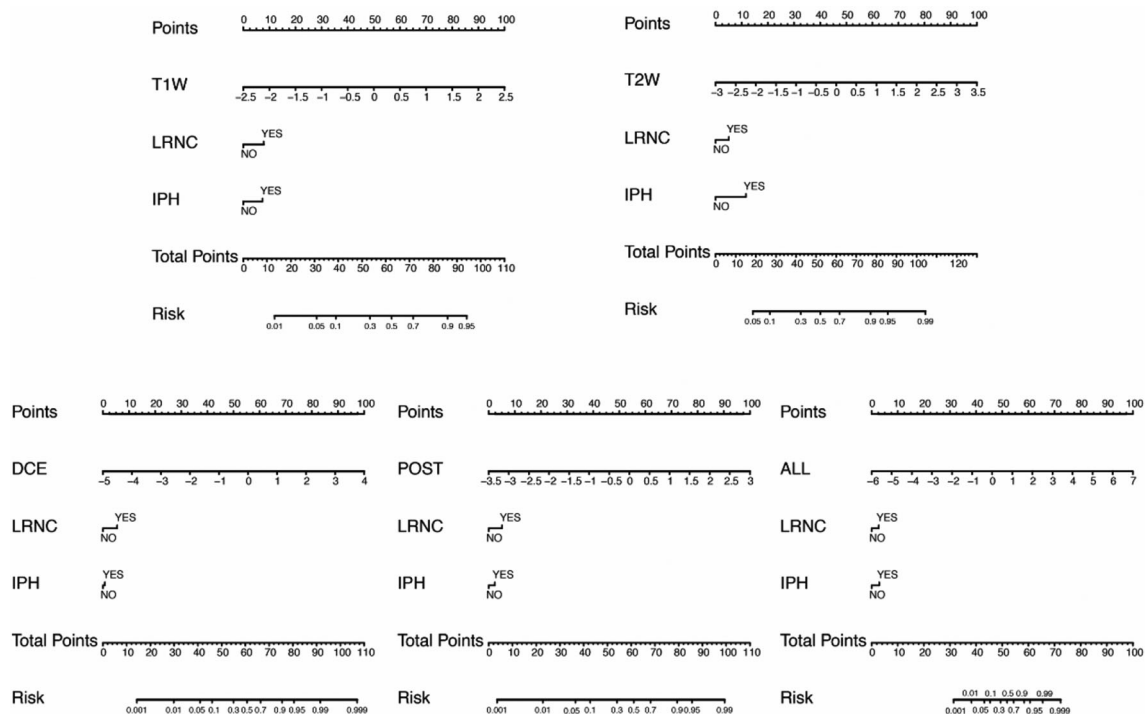
Fig. 3 A nomogram integrates the radiomics scores and traditional features of the training sets. The probability scoring of the carotid plaque being symptomatic is marked on each axis and increases from the left to right. The following is an example of how to calculate the total points of a plaque on T1W and predict its risk: a carotid plaque with LRNC but no IPH receives $7.5 + 0 = 7.5$ points from traditional features. A radiomics score of 2 corresponds to 90. Therefore, this plaque is scored 97.5 on the nomogram, which indicates a risk of over 95% of exhibiting symptoms. IPH, intraplaque hemorrhage; LRNC, lipid-rich necrotic core; DCE, dynamic contrast-enhanced sequence; POST, post-contrast delayed sequence; All, all features including T1WI, T2WI, DCE, and POST
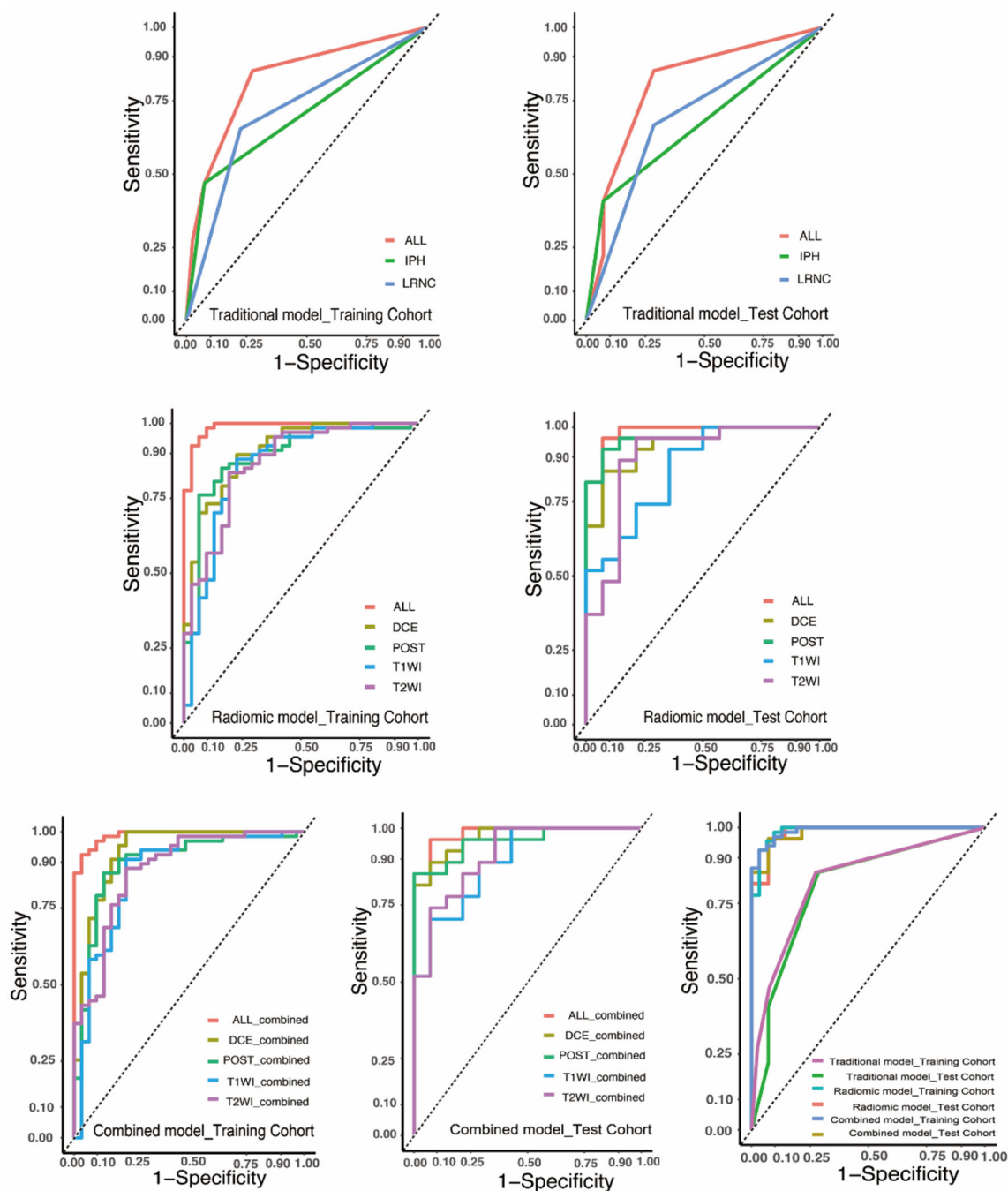
Fig. 4 Receiver operating characteristic (ROC) curves of all the models (traditional model, radiomics model—high-risk plaque MRI-based model (HRPMM) and combined model) in the training and test cohorts respectively. The ROC curves of the radiomics model and combined model outperform those of the traditional model in both the training (AUC, 0.988/0.989 vs. 0.825) and test (AUC, 0.984/0.986 vs. 0.804) cohorts. All, all features of each model; DCE, dynamic contrast-enhanced sequence; POST, post-contrast delayed sequence; IPH, intraplaque hemorrhage; LRNC, lipid-rich necrotic core

radiomics features from conventional plaque MRI and used the HRPMM to differentiate symptomatic carotid plaques from asymptomatic ones. The model consists of 33 radiomics features after optimization with LASSO and exhibits excellent diagnostic performance. With HRPMM, the risk score of each plaque could be computed, and the high-risk plaques could be identified. Additionally, the radiomics model shows an improved diagnostic performance compared with the traditional model, especially in specificity.

We found that independent radiomics features from 4 sequences were different, because different signal characteristics in various sequences were determined by different pathophysiological features. For example, the high signal on pre-contrast T1W possibly represents

IPH, while the high signal on post-contrast T1W may be attributed to the contrast uptake by neovascularization and inflammation. In the 33 final features, only sphericity, i.e., a shape feature, appeared in the four sequences' final screening results (see Appendix). It implies that sphericity may be the most important feature to delineate the morphology of the plaques. In both the training and test cohorts, the contrast-enhanced images from either the DCE or post-contrast delayed sequence demonstrated the highest AUC values. After combining all the radiomics features from four sequences, the AUC values were further improved in both cohorts. However, the diagnostic performance of the combined model was not significantly improved compared to the radiomics model alone. This could be explained by the relative weights of the radiomics versus traditional model, and the combined model was weighted heavily towards the radiomics features which produced better performances (Fig. 3). This comparison suggests that the traditional qualitative indicators might be covered, if not replaced, by quantitative descriptions by radiomics features. It further points to the potential of a more standardized diagnostic process based on objective quantitation. The reliability of our results was validated by the corrected AUCs after randomly sampling the training and test cohorts.

A number of studies have found certain carotid plaque features, such as IPH and LRNC, that were associated with an increased risk of plaque rupture and distal brain embolization. Measurements of stenosis, plaque burden, and enhancement ratio may also be predictive of future ipsilateral carotid symptoms. However, radiomics can provide reader-independent quantitative data [5] that are not readily apparent or are too numerous for an individual radiologist to assess visually. Radiomics contains richer information than traditional features; for example, IPH is a marker of high-risk carotid plaques, but most previous studies were qualitative identification in which the quantitative information about signal intensity, volume/shape, and the complicated distribution of IPH was lacking. That is why our HRPMM model was superior to traditional features in the classification of the high-risk carotid plaques.

To our knowledge, this study is the first investigation of high-risk carotid plaques with multi-contrast MRI using the radiomics approach and machine learning. A previous CT study [11] used discrete wavelet transform and texture features to classify carotid plaques with an accuracy of 88%, sensitivity of 90.2%, and specificity of 86.5%. Texture analysis was also successfully applied in ultrasound studies to improve the identification of symptomatic carotid plaques [10, 26]. Recently, a study [12] using radiomics texture analysis on MRI accurately distinguished symptomatic basilar

artery plaques with an excellent AUC of 0.936, while clinical imaging features alone had an AUC of 0.833. Based on these prior studies supporting the use of radiomics analysis to improve risk estimates, we further developed a MRI-based radiomics model to classify carotid plaques. Compared with previous reports, our radiomics model contained not only texture features but also other first-, second-, and higher-order statistics, all together contributing to the higher diagnostic accuracy of this model.

This study has the following limitations. The first was its relatively small sample size; especially in the test cohort, a larger data set is needed to evaluate this prediction model in the future. Secondly, ROIs were manually segmented, not yet fully automated, despite the excellent reproducibility. Thirdly, our traditional model only included two final radiological characteristics (IPH and LRNC), because all the relevant imaging features in relation to stroke risk were too mutually correlated so that they might be eliminated by multivariate analysis [18]. Fourthly, because of the indistinct boundary of the plaque on TOF, we did not perform radiomics analysis on it. Fifthly, the radiomics analysis was done on the slice with the largest plaque area. 3D analysis from whole image slices was not used because of the time restriction.

Conclusions

Radiomics analysis and machine learning of carotid plaques on MRI can accurately distinguish symptomatic from asymptomatic plaques. The radiomics model is better in the detection of high-risk plaques than the traditional model. Radiomics analysis has the greatest benefit of providing quantitative variables from the already-acquired imaging data to improve diagnostic performance beyond conventional evaluations. Prospective studies are needed to further examine the ability of HRPMM for predicting stroke risks.

Compliance with ethical standards

Guarantor The scientific guarantor of this publication is Jiang Lin.

Conflict of interest The authors of this manuscript declare no relationships with any companies whose products or services may be related to the subject matter of the article.

Statistics and biometry Zhang Qingwei and Zhang Ranying did statistical analysis.

Informed consent Written informed consent was obtained from all subjects (patients) in this study.

Ethical approval Institutional Review Board approval was obtained.

Methodology
- Retrospective
- Diagnostic or prognostic study
- Performed at one institution

References

1. Ooi YC, Gonzalez NR (2015) Management of extracranial carotid artery disease. Cardiol Clin 33:1–35

2. Naghavi M, Libby P, Falk E et al (2003) From vulnerable plaque to vulnerable patient: a call for new definitions and risk assessment strategies: part I. Circulation 108:1664–1672

3. Redgrave JN, Lovett JK, Gallagher PJ, Rothwell PM (2006) Histological assessment of 526 symptomatic carotid plaques in relation to the nature and timing of ischemic symptoms: the Oxford plaque study. Circulation 113:2320–2328

4. Zhou T, Jia S, Wang X et al (2019) Diagnostic performance of MRI for detecting intraplaque hemorrhage in the carotid arteries: a meta-analysis. Eur Radiol 29:5129–5138

5. Gillies RJ, Kinahan PE, Hricak H (2016) Radiomics: images are more than pictures, they are data. Radiology 278:563–577

6. Segal E, Sirlin CB, Ooi C et al (2007) Decoding global gene expression programs in liver cancer by noninvasive imaging. Nat Biotechnol 25:675–680

7. Coroller TP, Grossmann P, Hou Y et al (2015) CT-based radiomic signature predicts distant metastasis in lung adenocarcinoma. Radiother Oncol 114:345–350

8. Li W, Zhang L, Tian C et al (2019) Prognostic value of computed tomography radiomics features in patients with gastric cancer following curative resection. Eur Radiol 29:3079–3089

9. Wan L, Zhang C, Zhao Q et al (2019) Developing a prediction model based on MRI for pathological complete response after neo-adjuvant chemoradiotherapy in locally advanced rectal cancer. Abdom Radiol (NY) 44:2978–2987

10. Kakkos SK, Stevens JM, Nicolaides AN et al (2007) Texture analysis of ultrasonic images of symptomatic carotid plaques can identify those plaques associated with ipsilateral embolic brain infarction. Eur J Vasc Endovasc Surg 33:422–429

11. Acharya UR, Sree SV, Mookiah MRK et al (2013) Computed tomography carotid wall plaque characterization using a combination of discrete wavelet transform and texture features: a pilot study. Proc Inst Mech Eng H 227:643–654

12. Shi Z, Zhu C, Degnan AJ et al (2018) Identification of high-risk plaque features in intracranial atherosclerosis: initial experience using a radiomic approach. Eur Radiol 28:3912–3921

13. Barnett HJM, Taylor DW, Haynes RB et al (1991) Beneficial effect of carotid endarterectomy in symptomatic patients with high-grade carotid stenosis. N Engl J Med 325:445–453

14. Moseley ME, Kucharczyk J, Mintorovitch J et al (1990) Diffusion-weighted MR imaging of acute stroke: correlation with T2-weighted and magnetic susceptibility-enhanced MR imaging in cats. AJNR Am J Neuroradiol 11:423–429

15. Azizyan A, Sanossian N, Mogensen MA, Liebeskind DS (2011) Fluid-attenuated inversion recovery vascular hyperintensities: an important imaging marker for cerebrovascular disease. AJNR Am J Neuroradiol 32:1771–1775

16. Takaya N, Yuan C, Chu B et al (2006) Association between carotid plaque characteristics and subsequent ischemic cerebrovascular events: a prospective assessment with MRI–initial results. Stroke 37:818–823

17. Zhao X, Hippe DS, Li R et al (2017) Prevalence and characteristics of carotid artery high-risk atherosclerotic plaques in Chinese patients with cerebrovascular symptoms: a Chinese atherosclerosis risk evaluation II study. J Am Heart Assoc 6:e005831

18. Howard DP, van Lammeren GW, Rothwell PM et al (2015) Symptomatic carotid atherosclerotic disease: correlations between plaque composition and ipsilateral stroke risk. Stroke 46:182–189

19. Yuan C, Kerwin WS, Ferguson MS et al (2002) Contrast-enhanced high resolution MRI for atherosclerotic carotid artery tissue characterization. J Magn Reson Imaging 15:62–67

20. Yu JH, Kwak HS, Chung GH, Hwang SB, Park MS, Park SH (2015) Association of intraplaque hemorrhage and acute infarction in patients with basilar artery plaque. Stroke 46:2768–2772

21. Qian Z, Li Y, Wang Y et al (2019) Differentiation of glioblastoma from solitary brain metastases using radiomic machine-learning classifiers. Cancer Lett 451:128–135

22. Zhang L, Dong D, Li H et al (2019) Development and validation of a magnetic resonance imaging-based model for the prediction of distant metastasis before initial treatment of nasopharyngeal carcinoma: a retrospective cohort study. EBioMedicine 40:327–335

23. Kim SM, Kim Y, Jeong K, Jeong H, Kim J (2018) Logistic LASSO regression for the diagnosis of breast cancer using clinical demographic data and the BI-RADS lexicon for ultrasonography. Ultrasonography 37:36–42

24. Xie H, Ma S, Wang X, Zhang X (2020) Noncontrast computer tomography-based radiomics model for predicting intracerebral hemorrhage expansion: preliminary findings and comparison with conventional radiological model. Eur Radiol 30:87–98

25. Fluss R, Faraggi D, Reiser B (2005) Estimation of the Youden index and its associated cutoff point. Biom J 47:458–472

26. Huang X, Zhang Y, Qian M et al (2016) Classification of carotid plaque echogenicity by combining texture features and morphologic characteristics. J Ultrasound Med 35:2253–2261